

Article

Assessment of the Thermomechanical Behavior and Microstructure of AA 7075-T6 Aluminum Alloy Lap Joints at Optimal Predicted FSW Process Parameters

Oumayma Toumi ¹, Romdhane Ben Khalifa ¹, Alessia Teresa Silvestri ² , Ridha Ennetta ¹ , Fabio Scherillo ² 
and Umberto Prisco ^{2,*} 

¹ Mechanical Modelling, Energy & Materials, National School of Engineers, Gabes University, Zrig, Gabes 6029, Tunisia; oumayma.toumi@enig.rnu.tn (O.T.); romdhane.khalifa@ensit.rnu.tn (R.B.K.); ridha.ennetta@issig.rnu.tn (R.E.)

² Department of Chemical, Materials and Industrial Production Engineering, University of Naples Federico II, 80125 Naples, Italy; alessiateresa.silvestri@unina.it (A.T.S.); fabio.scherillo@unina.it (F.S.)

* Correspondence: umberto.prisco@unina.it

Abstract: The lap joints of AA 7075-T6 aluminum alloy were assembled using the friction stir welding (FSW) technique. Experimental studies were performed to characterize the thermomechanical properties of these welds. The main goal of this research was to comprehensively assess the thermomechanical behavior of AA 7075-T6 aluminum alloy under FSW conditions. Tests were carried out at a tool rotational speed of 1320 rpm and at two advancing speeds of 70 mm/min and 120 mm/min, selected based on a previous study aiming to optimize the heat input during the FSW process. The experimental investigations involved the characterization of temperature profiles during welding, mechanical properties such as microhardness and tensile strength, and microstructure examination at the two advancing speed conditions. This study revealed that the welding speed has an obvious influence on the material thermal behavior during the FSW process. Indeed, the peak temperature obtained with a lower welding speed (70 mm/min) was higher by almost 10% compared to that obtained with a higher speed (120 mm/min). Moreover, by increasing the welding speed, the mechanical characteristics, such as microhardness and tensile strength, were increased by almost 5% for the mean microhardness and 6% for the ultimate tensile strength. Additionally, the microstructure examination demonstrated that, by decreasing the welding speed, more interaction between the tool and the material is observed, resulting in a deeper stir zone due to increased heat dissipation downwards into the material, affecting the thermal profile and influencing the resulting mechanical properties of the welded joint.

Keywords: FSW; AA 7075-T6 aluminum alloy; lap joint; microstructure; thermomechanical properties



Citation: Toumi, O.; Khalifa, R.B.; Silvestri, A.T.; Ennetta, R.; Scherillo, F.; Prisco, U. Assessment of the Thermomechanical Behavior and Microstructure of AA 7075-T6 Aluminum Alloy Lap Joints at Optimal Predicted FSW Process Parameters. *Metals* **2024**, *14*, 839. <https://doi.org/10.3390/met14080839>

Academic Editors: Masahiro Fukumoto and Hardy Mohrbacher

Received: 22 May 2024

Revised: 4 July 2024

Accepted: 16 July 2024

Published: 23 July 2024



Copyright: © 2024 by the authors. Licensee MDPI, Basel, Switzerland. This article is an open access article distributed under the terms and conditions of the Creative Commons Attribution (CC BY) license (<https://creativecommons.org/licenses/by/4.0/>).

1. Introduction

Friction stir welding (FSW) is an advanced friction-based welding technique that originated in the early 1990s [1]. Unlike traditional fusion welding methods that involve melting and solidifying the base materials, FSW is a friction-based welding method that joins materials through mechanical deformation. It is particularly well suited for welding high-strength and heat-sensitive materials like aluminum alloys, which tend to lose their mechanical properties when subjected to traditional fusion welding [2]. Compared to fusion welding methods, FSW produces welds with superior mechanical properties, including higher strength and fatigue resistance, due to the solid-state joining process [3].

In FSW, a specifically designed revolving tool with a pin and shoulder is installed between the two pieces of material to be linked [4]. The tool is then rotated at high speeds while simultaneously traversing along the joint line. This rotation and movement causes frictional heat generation, which softens the material without melting it. The softened

material is mechanically stirred by the rotating tool, forming a high-quality, defect-free weld joint. FSW provides multiple benefits compared to conventional welding techniques, such as superior material behavior, reduced distortion, minimal porosity, and the capability to weld materials that are typically difficult to fuse [5]. FSW is employed in diverse industrial applications, involving the aviation, navy, automotive, construction, and other industries, where the need for strong, lightweight, and high-quality welds is paramount.

During recent years, the FSW technique has been the subject of several research studies aiming to optimize FSW tool parameters. Hassanifard et al. [6] evaluated the tensile and fatigue responses of AA 7075-T6 lap joints. This material exhibited slightly improved tensile strength after undergoing the FSW process. Additionally, the fatigue lives were enhanced up to 2.5 times. Lunetto et al. [7] investigated how different tool shapes affect the lap joint friction stir welding (FSW) of titanium sheets. The work emphasized certain optimization strategies and tool-related considerations in FSW processes. Babu Rao et al. [8] employed stochastic analysis techniques to evaluate the variability in the tensile strength of the welded lap joints of AA 7075-T6; the lowest tensile strength was obtained for the weld realized by the straight cylindrical profiled tool. Additionally, the tensile strength was increased by increasing the tool rotational speed up to 2000 rpm. Balakrishnan et al. [9] evaluated friction stir welds prepared using AA7075-T6 aluminum alloy with controlled variations in pin imperfections. Torque measurements showed an increase in the volume of material stirred by the tool when increasing the welding pitch, proving the effectiveness of using this technique to simulate material adhesion to the tool. Ge et al. [10] analyzed the impact of pin length and welding speed on the quality of lap joints formed by friction stir welding using dissimilar aluminum alloys. The study revealed that both pin length and welding speed significantly influence the quality of the lap joints; longer pin lengths generally result in better joint formation, while higher welding speeds may lead to decreased joint quality due to insufficient material flow and mixing.

Yuvaraj et al. [11] underscored the pivotal role of FSW tool parameter optimization in joining aluminum alloys of different compositions of type AA6061 and AA7075-T651. By employing the Taguchi technique, they identified the optimal combination of parameters for achieving welds characterized by enhanced strength and reduced defects. The significance lies in demonstrating the critical importance of selecting and optimizing FSW tool parameters for reliable and high-quality welds in dissimilar aluminum alloys.

Other studies were interested in the mechanical behavior and microstructure of FSW joints. Abolusoro et al. [12] delved into the evaluation of AA 7075 aluminum alloy welded lap joints using FSW. The primary aim was to assess the weld quality, mechanical properties, and microstructure by systematically varying the welding factors, including tool dimensions and design, traverse, and rotational speeds. The findings provided valuable insights for optimizing FSW parameters, particularly in achieving high-quality welded joints made of AA 7075 aluminum alloy. Kubit et al. [13,14] analyzed the mechanisms leading to mechanical behavior in overlap joints produced by FSW. By identifying the specific failure modes and underlying causes, including crack initiation at the weld interface, crack growth along the nugget periphery, and eventual joint separation, factors such as welding parameters, joint geometry, and material properties were found to significantly influence performance. Microstructural analysis indicates that microstructural features, such as grain morphology and precipitate distribution, play a crucial role in determining fatigue resistance.

AA 7075 T6 aluminum alloy stands out as a popular selection for friction stir welding (FSW) due to its unique combination of strength and lightweight characteristics. Renowned for its high strength-to-weight ratio and heat-treatable properties, this alloy is extensively used across various industries, particularly in aerospace and aviation [15]. Lap joints provide easier access for the FSW tool to traverse along the joint line and have the potential for more uniform material flow and mechanical properties compared to other joints such as butt joints. This accessibility facilitates the experimental setup and allows for more controlled and consistent welding conditions [16].

The AA 7075 T6 material has been extensively studied under FSW conditions. Most of these studies focused on investigating the effect of FSW parameters such as the rotational and advancing speeds, the tool geometry, and the joint type on the mechanical properties of the material. However, few studies have focused on optimizing this process by considering the thermal effect, which plays a crucial role in the FSW results.

The current study is a first attempt to optimize the FSW conditions of the AA7075-T6 lap joint, based on the heat generation during welding. This study focuses on determining the effects of specific welding speeds on the thermomechanical properties of the material.

Therefore, the primary goal of the current research was to experimentally assess the effects of FSW process parameters on the lap joint thermomechanical properties of the commonly used aluminum alloy AA 7075-T6. The temperature evolution, the stress–deformation curves, the hardness profiles, and the microstructure of the welded joint were measured at optimal advancing (welding) speeds. These speeds were selected based on a prior investigation focused on predicting the optimal FSW process parameters by optimizing the heat input during welding.

2. Experimental Set-Up

The experimental set-up consists of a welding tool mounted in a milling machine and two flat workpieces each measuring 200 mm × 100 mm × 2 mm. The welding tool is made from AISI H13 structural steel, which has been demonstrated to be effective for the FSW of aluminum alloys. The FSW process was employed to assemble two AA7075-T6 plates using the lap joint configuration (Figure 1).

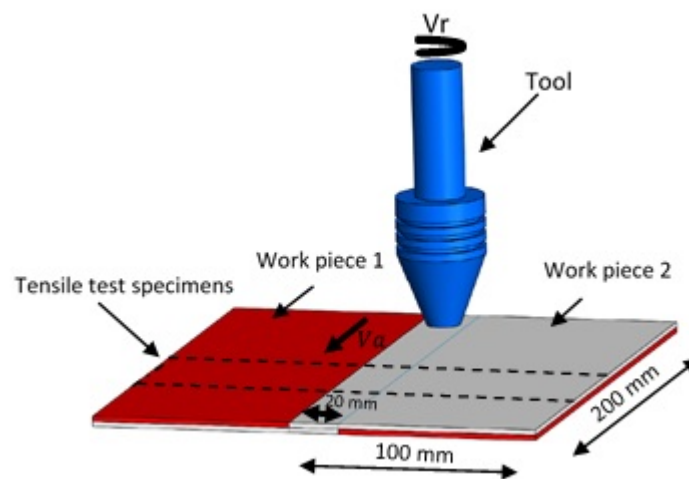


Figure 1. FSW lap joint configuration.

The sheet metal surfaces were meticulously cleaned to eradicate contaminants such as dirt and oxides. Then, the surfaces were preheated to achieve the optimal welding temperature, thereby reducing thermal gradients across the joint. Finally, the sheet metal pieces were collaboratively clamped with two holding wedges added to conserve the linearity securely to prevent any potential movement or misalignment during welding.

The mechanical behavior and average composition of AA7075-T6 are detailed in Tables 1 and 2.

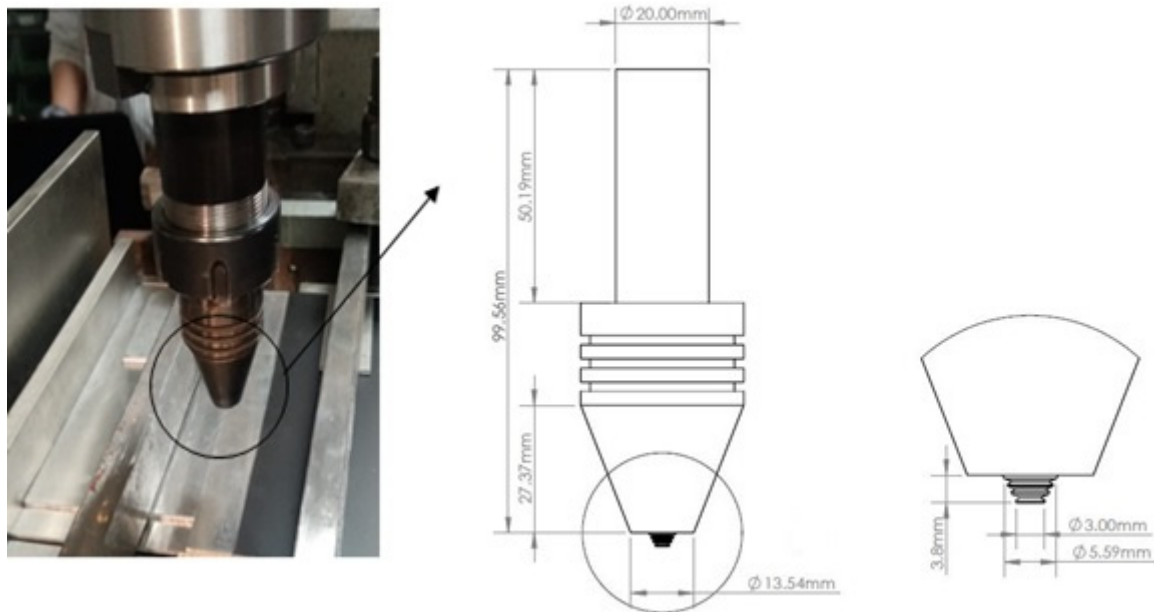
Table 1. Average composition (weight %) of the welded material. Reprinted from ref. [17].

| AA 7075-T6 | | | | | | | | |
|------------|---------|------|------|------|-------|------|------|-------|
| Cr | Al | Fe | Mg | Zn | Mn | Si | Cu | Ti |
| 0.029 | Balance | 0.61 | 2.04 | 5.11 | 0.014 | 0.33 | 1.11 | 0.027 |

Table 2. Mechanical behavior of the aluminum alloys. Reprinted from ref. [17].

| Aluminum Alloy | Yield Stress (MPa) | Elongation (%) | UTS (MPa) |
|----------------|--------------------|----------------|-----------|
| AA7075-T6 | 485 | 11 | 568 |

This tool had a cylindrical threaded shape with a 20 mm diameter, a 6 mm pin diameter, and a left-threaded cylindrical pin profile with a 1 mm pitch (Figure 2). The tool was tilted backwards by 2°.

**Figure 2.** Geometrical characteristics of the FSW tool.

2.1. Prediction of Optimal FSW Process Conditions

The welding speeds were chosen according to a previous study aiming to predict the appropriate FSW process parameters, which were determined according to the optimization of the heat input during the process.

Yi et al. [18] predicted the appropriate FSW process factors based on the optimization of the heat input during welding. They conducted a comprehensive study and established a regression equation relating welding parameters and heat input. This equation was used in the current study, considering optimized minimum and maximum heat input values, to determine the welding speeds, as follows:

$$HI = 7.2 \times V^{-0.80} \times N^{-0.10} \times D^{0.55} \times d^{0.45} \times h^{0.30} \times \lambda^{0.40} \quad (1)$$

where HI , D , V , h , N , λ , and d represent the heat input (J/mm), probe diameter (mm), advancing speed (mm/s), probe length (mm), rotating speed (rad/s), thermal conductivity of the workpiece (W/mK), and shoulder diameter (mm), respectively.

The tool parameters are $D = 13$ mm, $d = 3$ mm, $h = 3$ mm. The AA 7075-T6 thermal conductivity is $\lambda = 130$ W/mk [19].

According to Yi et al. [18], $HI_{min} = 423.89$ J/mm and $HI_{max} = 688.6$ J/mm.

The chosen rotational speed is 1320 rpm, giving $N = 141.37$ rad/s [20,21].

Based on Equation (1), the optimal minimum and maximum welding speeds are as follows:

$$V_{max} = 1.984 \text{ mm/s} \approx V = 120 \text{ mm/min};$$

$$V_{min} = 1.083 \text{ mm/s} \approx V = 70 \text{ mm/min}.$$

The impacts of these two advancing speeds on the thermomechanical behavior and microstructure of the AA 7075-T6 lap joints were experimentally investigated.

2.2. Temperature Measurement

Temperature measurements were taken during FSW on both the workpieces and the FSW tool. A digital K-type thermocouple laser thermometer was utilized to measure these temperatures. In order to evaluate how welding speed affects the temperature distribution throughout the weld, measurements were conducted at a distance of 0.5 mm from the shoulder surface and both the probe tip and the shoulder surface. Stir zone temperatures were measured close to the transition from the probe to the shoulder, as this is considered the hottest point inside the weld [22]. The thermometer laser beam was pointed at the weld center on the work piece and close to the rotating pin area. The time variations in the temperature were recorded for the two welding speeds: V_{min} (Hot) and V_{max} (Cold).

2.3. Test Specimen Preparation

The test samples were extracted from the welds executed at the two welding speeds. To facilitate the analysis process, the samples were mounted using a conductive thermosetting resin, as presented in Figure 3. Subsequently, these mounted samples were placed on an abrasive disc and polished using polycrystalline diamond powder, ranging from 0.05 to 9 μm , on a cloth disc.

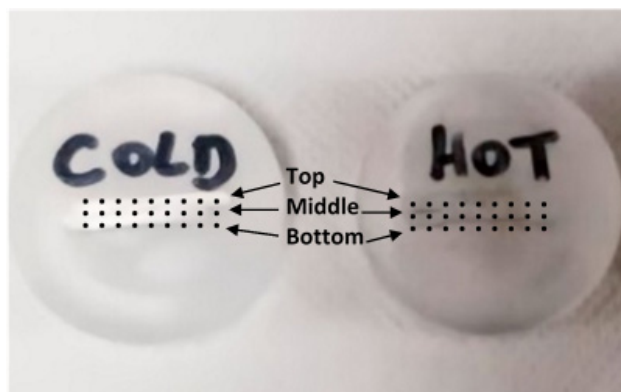


Figure 3. Test samples for microstructure and microhardness tests.

To be able to observe the microstructure that formed along the FSW joint, measurements were taken under the two advancing speed conditions. The polished test samples were immersed in an aqueous hydrofluoric acid solution. The analysis was initiated with optical microscopy using a Leica DCM3D (Wetzlar, Germany) confocal microscope to detect any potential internal defects. Subsequently, with the aim of analyzing the weld surface microstructure, scanning electron microscopy using a Hitachi TM3000 (Tokyo, Japan) was employed.

Additionally, Vickers microhardness tests were conducted using a LEICA VMHT AUTO (Wetzlar, Germany) machine according to the ASTM E384-22 standard [23] under an indenter load of 200 g. Specifically, hardness measurements were conducted at three locations, spaced approximately 2 mm apart, across the cross-section of the welded line, as illustrated in Figure 4.

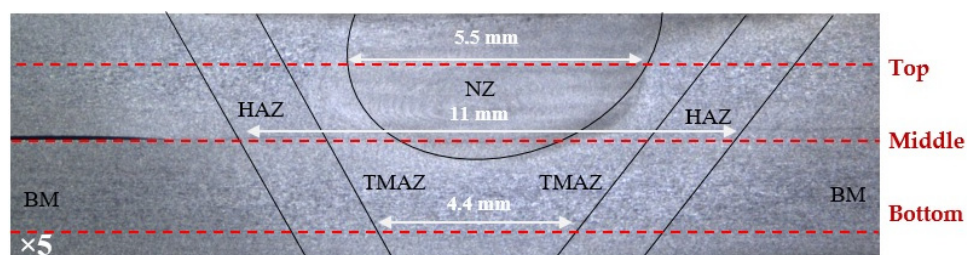


Figure 4. Schematic diagram for microhardness traverse position.

Moreover, tensile tests were performed using a Galdabini QUASAR 50 (Cardano al Campo, Italy) following the ASTM E8 standard [24] on lap joint samples of 2 mm thickness for each part, as depicted in Figure 5. During these tensile tests, a constant tensile test speed of 1.3 mm/min [25] was selected. Firstly, the lap joint was securely fixed or clamped to ensure stability during the extraction process. Then, a cutting tool, i.e., a water jet cutting machine, was used to precisely cut through the joint, separating it into individual specimens. Care was taken to ensure that the specimens were extracted in a manner that preserved their integrity and dimensions, minimizing any potential distortion or damage to the weld zone.

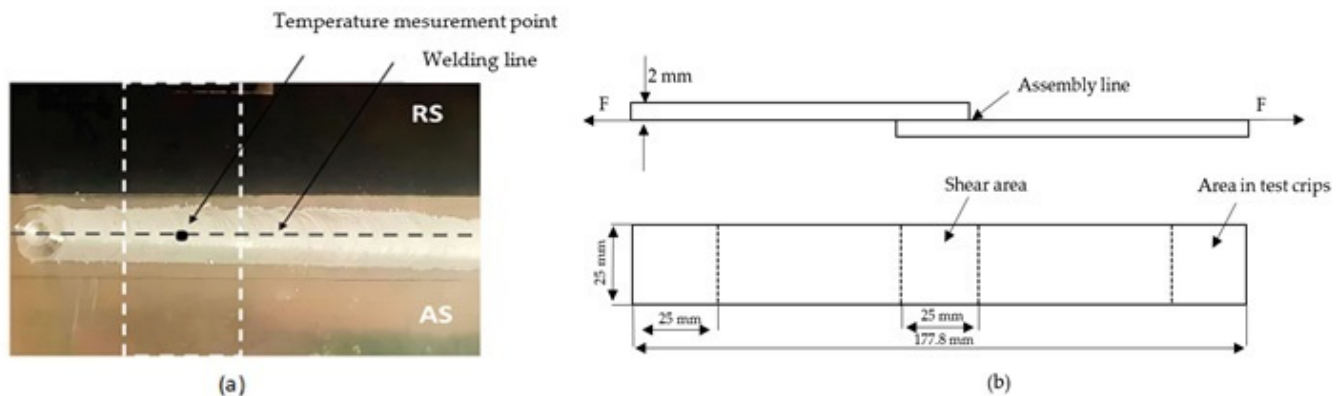


Figure 5. Form (a) and dimensions (b) of tensile test specimens.

Various tensile strength specimens were extracted from each weld executed at the chosen welding speed. The average value was then calculated.

3. Results and Discussion

3.1. Temperature

The temperature evolution along FSW was determined in real time using a laser thermometer along the weld line behind the tool. Temperature measurements were initiated at the beginning of welding to capture the initial heating stages, and the temperature evolution in point measurement along the FSW process was determined in real time.

Figure 6 illustrates the time variations in the temperature of the AA7075-T6 lap joint welds under the two welding speed conditions, 70 mm/min and 120 mm/min, labeled hot and cold welding, respectively. It is clear that, in both cases, the temperature peaks were obtained after a certain time and near the end of the welding process. This can be ascribed to the heat accumulation resulting from the heat input during the tool advancement, which results in temperature rises. Increasing the welding speed significantly decreases the duration of high temperatures. This suggests that welding speed significantly influences the exposure time of the weld zone to high temperatures, primarily due to the shortened dwell time per unit length as the welding speed increases.

As shown in Figure 6, the temperature increases more quickly during cold welding as a result of the increased welding speed, reaching a value of about 433 K in approximately 50 s. However, in the case of hot welding, the peak temperature of almost 450 K was reached in more time, approximately 60 s. These results resemble those obtained by Nandan et al. [26]. In this last case, the higher value of peak temperature is due to the lower welding speed allowing for more residence time, which results in more friction interaction between the pieces and the tool and then providing more heat flux, as explained by Verma and Misra [27].

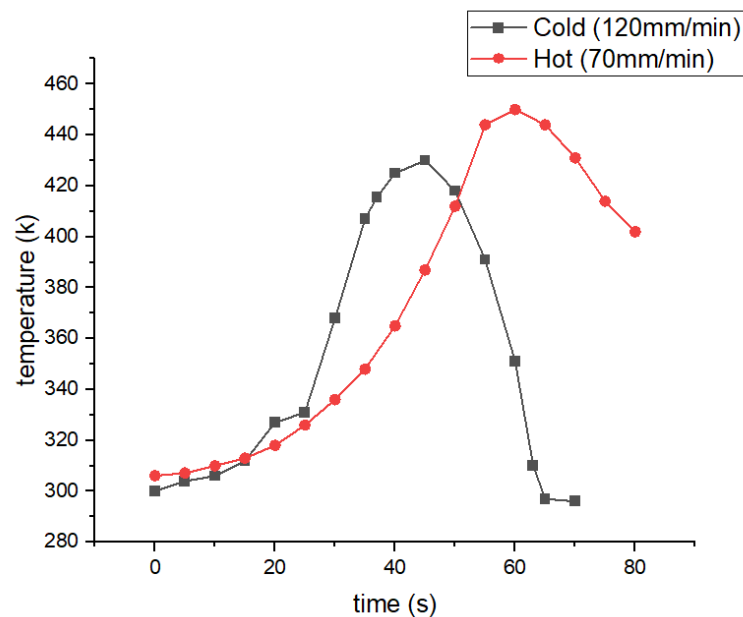


Figure 6. Temperature profiles along the hot and cold welding.

3.2. Microhardness

The Vickers bulk hardness tester was employed to assess the hardness values of the friction stir weld (FSW) joint specimens. Hardness measurements were taken equidistantly from both sides of the weld nugget zone (NZ).

Figure 7 gives the microhardness determined in the three zones (top, middle, and bottom) of the specimens described previously in Figure 3. It is noteworthy that the highest microhardness records were noted near the center of the NZ, gradually decreasing as one approaches the thermomechanical-affected zone (TMAZ) and then the heat-affected zone (HAZ). This trend remained consistent irrespective of the welding speeds.

The base metal (BM), especially in the middle and bottom zones, exhibited a maximum hardness of approximately 110 ± 5 HV, while the NZ material displayed a higher hardness of about 155 ± 2 HV, in the case of cold welding. The increased hardness in the NZ is caused by the disruption of significant primary grain structures caused by the stirring action produced by the rotation of the tool, as described by Nadikudi et al. [28]. However, in the thermomechanical-affected zone (TMAZ), the lower strain energy leads to plastic deformation, and recrystallization occurs partially and at a slower rate compared to the NZ. Consequently, this leads to the formation of coarse, uneven, and elongated grains, resulting in lower hardness than that in the NZ. Dong et al. [29] reported similar findings. Additionally, in the HAZ, the temperature input from the rotating tool is lower than in the TMAZ due to the distance from the NZ. This results in the formation of larger grains and, subsequently, lower hardness due to the annealing effect caused by the slower cooling rate.

Moreover, the hardness profile indicates that the hardness on the weld advancing side (AS) is marginally higher compared to the retreating side (RS). This variance can be ascribed to the increased heat input from the advancing side, caused by increased friction and shear forces. Consequently, this leads to enhanced grain refinement and increased hardness on the AS, as described by Verma and Misra [27].

As shown in Figure 7, it is evident that the variation in the welding speed influenced the hardness values. Irrespective of the welded joint region, the hardness increased with the welding speed increase. At low welding speeds, higher temperatures are reached, and larger grains are obtained, leading to lower hardness levels. However, at high welding speeds, lower temperatures are attained, resulting in smaller grains and higher hardness levels. The same explanation was given by Kumar et al. [30]. In the top zone, the peak values were detected on the left hand side due to the intensity of the forces involved in this

area, while the advancing side was generally less hard due to the relatively less intense interaction with the welding tool. In the middle zone, the curves exhibited twin peaks, indicating areas of localized hardness due to the combined effects of heat and mechanical deformation during the welding process. In the bottom zone, the peak values shifted to the right.

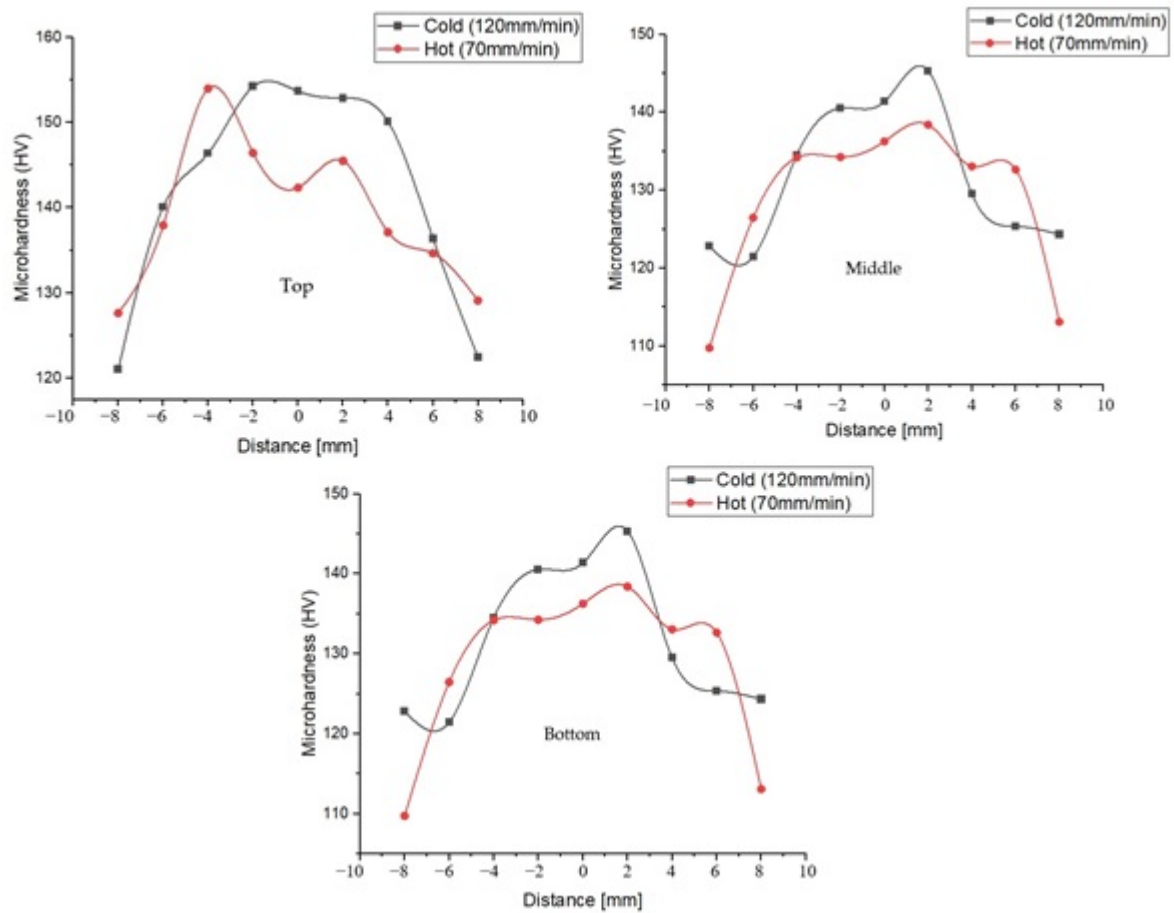


Figure 7. Microhardness profiles of the welded joints for hot and cold welding.

3.3. Tensile Test

Tensile strength tests were conducted using the Galdabini QUASAR 50, a universal testing machine. As mentioned previously, the samples were extracted from welds executed using different welding speeds. Figure 8 presents an example of fractured tensile specimens for cold and hot welding.



Figure 8. Fractured FSW lap joint specimens after tensile test for (a) cold welding and (b) hot welding.

Figure 9 presents the stress–strain curves obtained through tensile tests on AA 7075-T6 material subjected to both hot and cold welding processes. The tests were executed in the transversal direction of the welding line. The data illustrated in the graph reveal an interesting trend: despite the similarity in yield stress variations observed between both types of weld samples, there is a discernible disparity in the overall ductility. Specifically, the ductility of the hot-welded samples exhibits a reduction when compared to the cold-welded material. Hence, the elongation at break (fracture strain) increased from around

5.5% in the case of the hot-welded sample to around 5.9% in the case of the cold-welded sample, which represent an increase of more than 7% by increasing the welding speed from 70 mm/min to 130 mm/min. This decline in ductility for the hot-welded samples aligns with findings from Darzi Naghibi et al. [31] and Babu Rao [8], who previously reported a significant hardness mismatch in these particular welds. This phenomenon highlights the significant impact of process conditions on the mechanical behavior of the resulting joints, particularly in terms of ductility. These experimental findings corroborate the importance of considering ductility and hardness matching in welding processes, as highlighted by the comparison between hot and cold welding in this study. It is important to note that the material exhibits a rapid strain rate, indicating elastic deformation behavior due to alterations in atomic adhesion. This phenomenon contributes to material weakness and eventual fracture [32]. Conversely, materials with high toughness exhibit greater resistance to atomic dislocation, resulting in limited elastic deformation behavior. For instance, under conditions such as a rotational speed of 1320 rpm, the AA7075 T6 aluminum alloy demonstrated maximum tensile strengths of 170 MPa and 160 MPa, with a strain rate of 6% and 6.3%, at welding speeds of 70 mm/min and 120 mm/min, respectively. This is attributed to the alloy's inherent strength and ductility. Compared to the values obtained by Cabrini et al. [33] for the base material, FSW led to a decrease in stress by about 200 MPa. Increasing welding speeds also heightens the probability of residual stresses within the welded structure. Such stresses have the potential to compromise the material's integrity, rendering it more prone to cracking and failure.

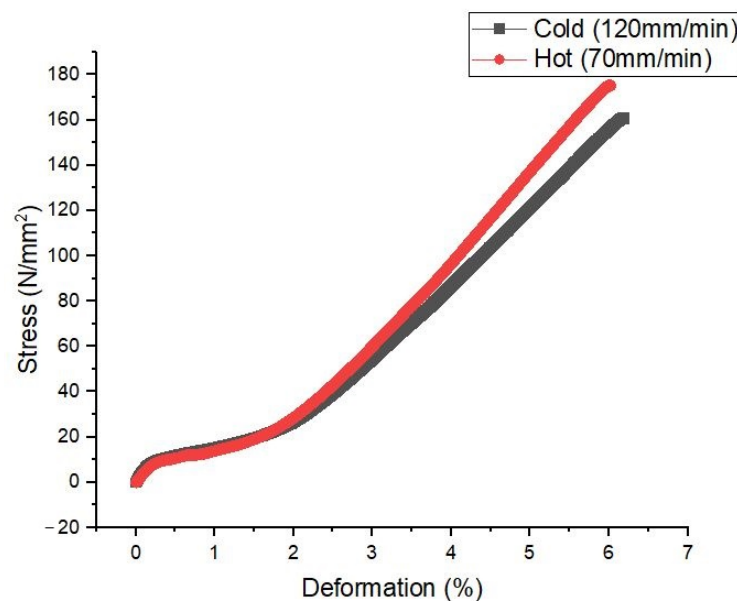


Figure 9. Stress–deformation curves for FSW samples obtained at various welding speeds.

3.4. Microstructure

The FSW microstructure was revealed through optical and scanning electron microscopes. Figures 10 and 11 present the micrographs of various regions of the joint under cold and hot welding conditions, respectively. The grain sizes (Figure 11) were measured by employing ImageJ 1.54i software.

Figure 10 offers insights into the metallurgical characteristics observed in the cross-sectional view. Upon macroscopic examination, no discernible flaws were detected in the analyzed joint. Notably, a substantial grain refinement is evident when comparing the microstructures of the base metal (BM) and the nugget zone (NZ). The BM structure, Figure 10c,i, typically comprises elongated grains, resembling those commonly found in rolled plates, with an average grain size of 15 to 20 μm . The NZ, Figure 10d, is described as the zone of the joint bead where full recrystallization has taken place as a result of the tool activity. This leads to the development of a finer grain microstructure in the NZ

(Figure 10e,f), with an average grain size of less than $14\ \mu\text{m}$, as depicted in Figure 11. The thermomechanical-affected zone (TMAZ) is the zone of the weld bead with deformed and extended grains indicating the direction of material movement in the FSW process. Adjacent to the nugget zone (NZ), the TMAZ undergoes plastic deformation while being exposed to elevated temperatures. However, this zone does not experience recrystallization. The conditions are inadequate to induce recrystallization. Instead, the grains in the thermomechanical-affected zone (TMAZ) are stretched, as illustrated in Figure 10a,g, aligning with the flow direction. This stretching causes a reduction in width and an extension in grain length, with a mean value of about $66\ \mu\text{m}$ to $75\ \mu\text{m}$, as illustrated in Figure 11. Fully recrystallized zones are noticeable in the center of the joint (Figure 10e). The boundary between the thermomechanical-affected zone (TMAZ) and the nugget zone (NZ) is evident in Figure 10b,e. However, there is significant material flow at the boundary between the NZ and TMAZ, with material rising from the bottom of the workpiece and descending from the surface. As a result, the demarcation between the NZ and TMAZ is diffuse and gradual. When examined at higher magnifications, it becomes apparent that the weld nugget displays fine grains that are equiaxed, while the TMAZ exhibits larger and elongated grains. Similar observations have been stated by Aydin et al. and Manikandan et al. [32,34]. They elucidated that the microstructure of the nugget zone (NZ) primarily arises from elevated temperatures and plastic deformation, resulting in dynamic recrystallization. Conversely, the microstructure of the thermomechanical-affected zone (TMAZ) is attributable to the combined effects of high stress and large strain, but without recrystallization.

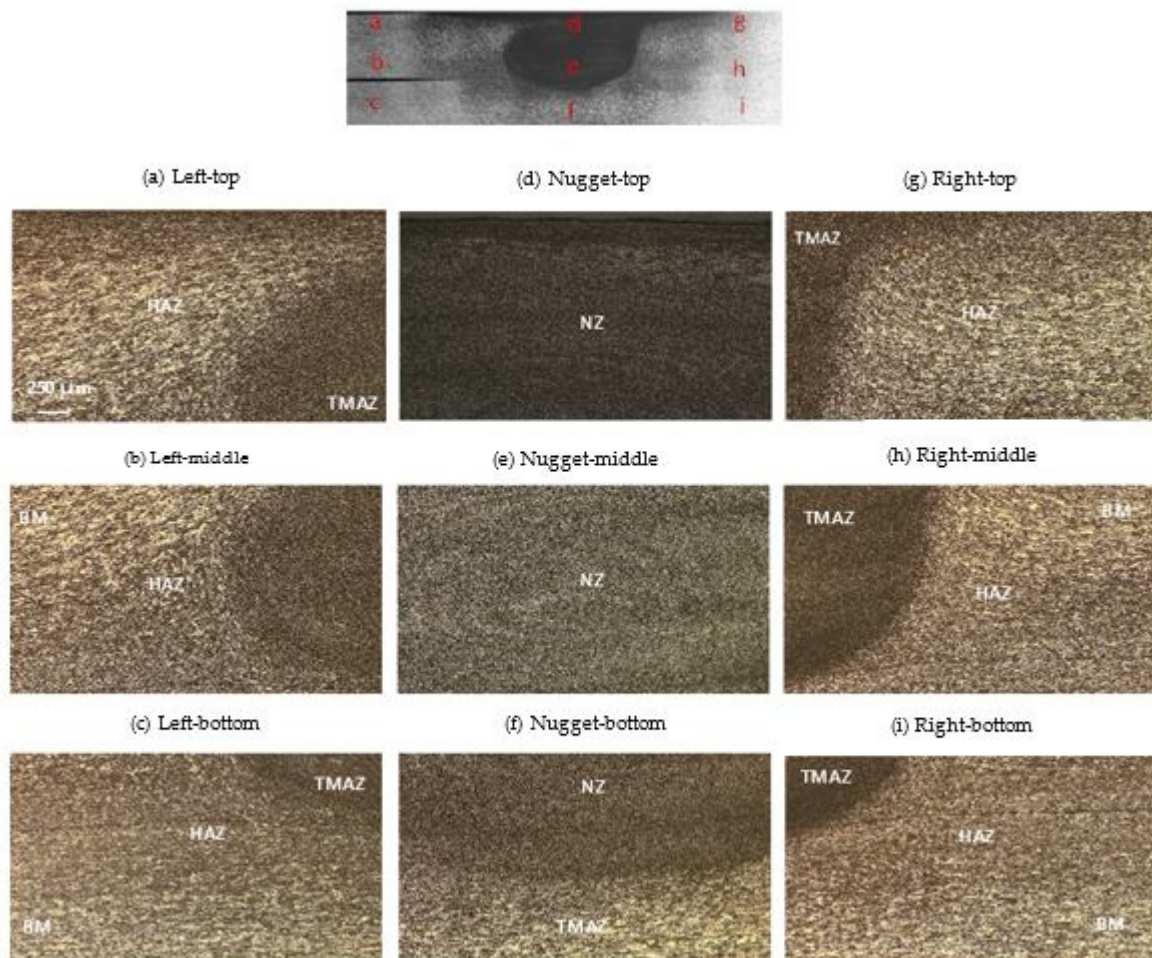


Figure 10. Optical and scanning electron micrographs of various zone of the joint under cold welding conditions.

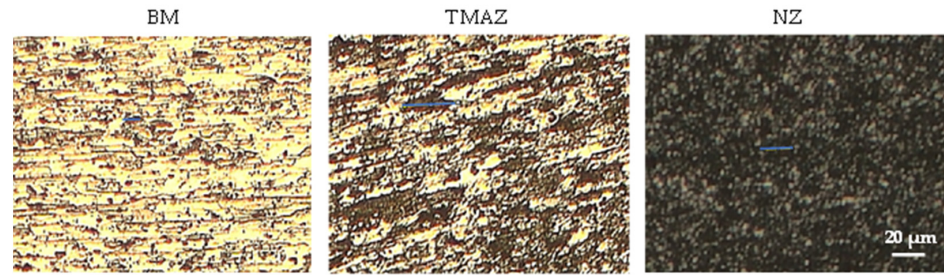


Figure 11. Grain size measurement using ImageJ for cold welding specimen.

In Figure 10b, the extremely fine tip, encircled by fully recrystallized AA7075-T6 grains, is discernible. Figure 10f points out two distinct areas: TMAZ and the stretched grains of the heat-affected zone (HAZ). At these magnifications, the heat-affected zone (HAZ) is difficult to identify due to its distinct distribution characteristics, as stated by Carlone et al. [35]. This particularity has been observed across various aluminum alloys.

Figure 10 shows that the tool has not been fully plunged. The pin is approximately 3.8 mm in length, while each sheet thickness is 2 mm. However, the image reveals that the stir zone has only marginally affected the bottom sheet. Conversely, Figure 12 illustrates a more pronounced plunge into the bottom sheet. This increased penetration suggests a greater interaction between the tool and the material, resulting in a deeper stir zone. The difference in the tool plunge between the two images influences the heat dissipation dynamics. When the tool makes a more severe plunge into the bottom sheet, as depicted in Figure 12, it facilitates enhanced contact and frictional forces between the tool and the material. Consequently, this intensified interaction leads to increased heat dissipation downwards into the material, affecting the thermal profile and influencing the resulting mechanical properties of the welded joint.

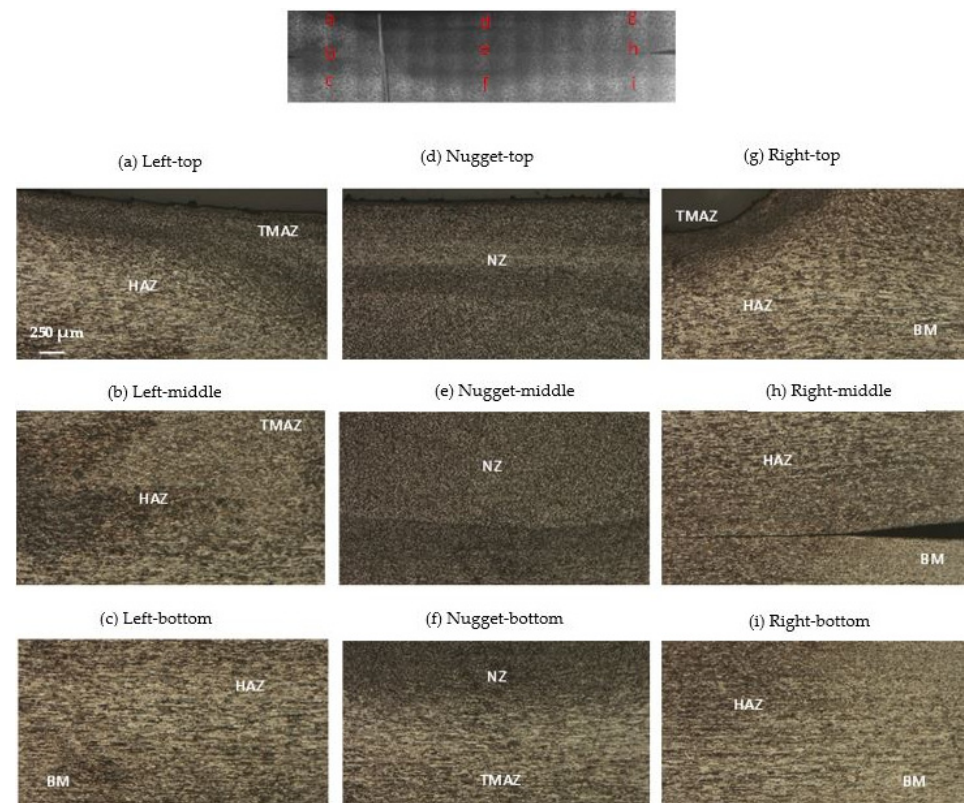


Figure 12. Optical and scanning electron micrographs of various zones of the joint under hot welding conditions.

The microstructure of the FSW lap joint under hot welding conditions (low advancing speed) is illustrated in Figure 12. The nugget zone (NZ) is clearly visible in Figure 12d,e, showcasing a distinct and continuous process of dynamic recrystallization. In contrast to cold welding, when utilizing hot friction stir welding (FSW), there is a rise in the grain size of the AA7075-T6 aluminum alloy, ranging from 20 μm to 25 μm , accompanied by a transformation to equiaxed shapes. Notably, coarser grains are identifiable, according to the findings of Topic et al. [36] and Sun et al. [37]. The temperature within the NZ reaches as high as 250 $^{\circ}\text{C}$, a level sufficient to induce overaging effects.

The micrographs in Figure 13 depict a trend where grain sizes tend to increase as the advancing speed of the tool decreases. In the heat-affected zone (HAZ) and in the thermomechanical-affected zone (TMAZ), where grains are solely influenced by heat, larger grains are observed with a mean size ranging from 68 μm to 79 μm . This phenomenon can be attributed to the substantial deformations caused by the mechanical effect of the tool at elevated temperatures during welding, as elucidated by Aliha et al. [38].



Figure 13. Grain size measurement using ImageJ for hot welding specimen.

4. Conclusions

This study examined the thermomechanical properties of friction stir welding (FSW) in lap joints of AA 7075-T6 aluminum alloy. Through extensive experimental investigations, temperature profiles during welding, mechanical properties, and microstructural alterations were scrutinized. The examination of the microstructure, microhardness, and tensile test behavior of grinding-blend-welded lap joints of AA7075-T6 aluminum alloy carried out under various process conditions—specifically, two advancing speeds—revealed the following findings:

- The lowest ultimate tensile strength of AA7075-T6 was obtained under hot welding conditions. The ultimate tensile strength decreased by decreasing the welding speed. This trend was also observed for microhardness. This is mainly attributed to the decline in the material's inherent strength and ductility due to the microstructure modification caused by the heat generated by the tool's welding speed.
- The FSW process parameters were evaluated via tensile test and hardness tests. Comparing the two welding speeds, at a rotational speed of 1320 rpm, the best parameters were obtained at a welding speed of 120 mm/min.
- The nugget zone (NZ) microstructure was characterized by extremely thin, completely reformed equiaxed grains, exhibiting the most significant refinement. In contrast, the thermomechanical-affected zone (TMAZ) consisted of highly distorted and partially recrystallized grain, caused by the elevated temperature and deformation applied by the welding tool. However, the heat-affected zone (HAZ) microstructure, characterized by overgrown grains, was similar to that of the base metal (BM), since the HAZ is only exposed to heat and not to deformations.
- As the welding speed decreased, the NZ grain size increased by a rate ranging from 25% to 33% induced by the overaging effects due to the high temperatures reached during hot welding.

- The ascending trend in TMAZ grain size at hot welding ($V_s = 70$ mm/min), with a rate ranging from 3% to 5%, compared to cold welding ($V_s = 120$ mm/min) shows that the generated heat played the main role in FSW rather than plastic deformation.

Author Contributions: Conceptualization, O.T., R.B.K. and R.E.; methodology, R.B.K. and F.S.; investigation, O.T., A.T.S. and F.S.; resources, F.S.; writing—original draft preparation, O.T.; writing—review and editing, A.T.S., R.E. and U.P.; visualization, R.B.K.; supervision, R.E. and U.P.; funding acquisition, U.P. All authors have read and agreed to the published version of the manuscript.

Funding: This research received no external funding.

Data Availability Statement: The raw data supporting the conclusions of this article will be made available by the authors on request.

Acknowledgments: The authors gratefully acknowledge the support of Sana Hmida, an English professor, in the language editing of the manuscript.

Conflicts of Interest: The authors declare no conflicts of interest.

References

1. Thomas, W.; Nicholas, E.; Needham, J.; Murch, M.; Temple-Smith, P.; Dawes, C. Friction Stir Butt Welding (The Welding Institute (TWI)). PCT World Patent Application WO 93/10935, 10 June 1993.
2. Xiao, X.; Mao, Y.; Wang, X.; Qin, D.; Fu, L. Effects of Curvature Direction on Friction Stir Welding Lap Joint of Aluminum Alloy “S” Curved Surface. *Int. J. Adv. Manuf. Technol.* **2023**, *125*, 4693–4705. [[CrossRef](#)]
3. Yaduwanshi, D.K.; Rao, C.R.M.; Naidu, S.R.M.; Sakharwade, S.G.; Sharma, S.; Khalkar, V.; Baskar, S.; Kaliyaperumal, G. Thermal Evaluation of Aluminum Welding: A Comparative Study of Friction Stir Welding (FSW), Plasma-Fsw, and Tungsten Inert Gas (TIG)-FSW Techniques. *Int. J. Interact. Des. Manuf. (IJIDeM)* **2024**, 1–13. [[CrossRef](#)]
4. Mirzaei, M.; Asadi, P.; Fazli, A. Effect of Tool Pin Profile on Material Flow in Double Shoulder Friction Stir Welding of AZ91 Magnesium Alloy. *Int. J. Mech. Sci.* **2020**, *183*, 105775. [[CrossRef](#)]
5. Alemdar, A.S.A.; Jalal, S.R.; Mulapeer, M.M.S. Influence of Friction Stir Welding Process on the Mechanical Characteristics of the Hybrid Joints AA2198-T8 to AA2024-T3. *Adv. Mater. Sci. Eng.* **2022**, *2022*, 7055446. [[CrossRef](#)]
6. Hassanifard, S.; Ghiasvand, A.; Varvani-Farahani, A. Fatigue Response of Aluminum 7075-T6 Joints through Inclusion of Al_2O_3 Particles to the Weld Nugget Zone during Friction Stir Spot Welding. *J. Mater. Eng. Perform.* **2021**, *31*, 1781–1790. [[CrossRef](#)]
7. Lunetto, V.; De Maddis, M.; Russo Spena, P. Similar and Dissimilar Lap Friction Stir Welding of Titanium Alloys: On the Elimination of the Hook Defect. *Int. J. Adv. Manuf. Technol.* **2023**, *126*, 3417–3435. [[CrossRef](#)]
8. Babu Rao, T. Stochastic Tensile Failure Analysis on Dissimilar AA6061-T6 with AA7075-T6 Friction Stir Welded Joints and Predictive Modeling. *J. Fail. Anal. Prev.* **2020**, *20*, 1333–1350. [[CrossRef](#)]
9. Balakrishnan, M.; Leitão, C.; Arruti, E.; Aldanondo, E.; Rodrigues, D. Influence of Pin Imperfections on the Tensile and Fatigue Behaviour of AA 7075-T6 Friction Stir Lap Welds. *Int. J. Adv. Manuf. Technol.* **2018**, *97*, 3129–3139. [[CrossRef](#)]
10. Ge, Z.; Gao, S.; Ji, S.; Yan, D. Effect of Pin Length and Welding Speed on Lap Joint Quality of Friction Stir Welded Dissimilar Aluminum Alloys. *Int. J. Adv. Manuf. Technol.* **2018**, *98*, 1461–1469. [[CrossRef](#)]
11. Yuvaraj, K.; Varthanan, P.A.; Haribabu, L.; Madhubalan, R.; Boopathiraja, K. Optimization of FSW Tool Parameters for Joining Dissimilar AA7075-T651 and AA6061 Aluminium Alloys Using Taguchi Technique. *Mater. Today Proc.* **2021**, *45*, 919–925. [[CrossRef](#)]
12. Abolusoro, O.P.; Akinlabi, E.T.; Kailas, S.V. Tool rotational speed impact on temperature variations, mechanical properties and microstructure of friction stir welding of dissimilar high-strength aluminium alloys. *J. Braz. Soc. Mech. Sci. Eng.* **2020**, *42*, 176. [[CrossRef](#)]
13. Kubit, A.; Bucior, M.; Wydrzyński, D.; Trzepieciński, T.; Pytel, M. Failure Mechanisms of Refill Friction Stir Spot Welded 7075-T6 Aluminium Alloy Single-Lap Joints. *Int. J. Adv. Manuf. Technol.* **2018**, *94*, 4479–4491. [[CrossRef](#)]
14. Kubit, A.; Trzepieciński, T.; Bochnowski, W.; Drabczyk, M.; Faes, K. Analysis of the Mechanism of Fatigue Failure of the Refill Friction Stir Spot Welded Overlap Joints. *Arch. Civ. Mech. Eng.* **2019**, *19*, 1419–1430. [[CrossRef](#)]
15. Garg, A.; Raturi, M.; Garg, A.; Bhattacharya, A. Microstructure Evolution and Mechanical Properties of Double-Sided Friction Stir Welding between AA6061-T6 and AA7075-T651. *CIRP J. Manuf. Sci. Technol.* **2020**, *31*, 431–438. [[CrossRef](#)]
16. Li, B.; Shen, Y. A Feasibility Research on Friction Stir Welding of a New-Typed Lap-Butt Joint of Dissimilar Al Alloys. *Mater. Des.* **2012**, *34*, 725–731. [[CrossRef](#)]
17. Ghiasvand, A.; Suksatan, W.; Tomków, J.; Rogalski, G.; Derazkola, H.A. Investigation of the Effects of Tool Positioning Factors on Peak Temperature in Dissimilar Friction Stir Welding of AA6061-T6 and AA7075-T6 Aluminum Alloys. *Materials* **2022**, *15*, 702. [[CrossRef](#)]
18. Yi, D.; Onuma, T.; Mironov, S.; Sato, Y.; Kokawa, H. Evaluation of Heat Input during Friction Stir Welding of Aluminium Alloys. *Sci. Technol. Weld. Join.* **2017**, *22*, 41–46. [[CrossRef](#)]

19. Ishak, M.; Noordin, N.; Shah, L. *Parametric Studies on Tensile Strength in Joining AA6061-T6 and AA7075-T6 by Gas Metal Arc Welding Process*; IOP Publishing: Bristol, UK, 2015; Volume 100, p. 012042. [[CrossRef](#)]
20. Meengam, C.; Sillapasa, K. Evaluation of Optimization Parameters of Semi-Solid Metal 6063 Aluminum Alloy from Friction Stir Welding Process Using Factorial Design Analysis. *J. Manuf. Mater. Process.* **2020**, *4*, 123. [[CrossRef](#)]
21. Azimzadegan, T.; Serajzadeh, S. An Investigation into Microstructures and Mechanical Properties of AA7075-T6 during Friction Stir Welding at Relatively High Rotational Speeds. *J. Mater. Eng. Perform.* **2010**, *19*, 1256–1263. [[CrossRef](#)]
22. Silva, A.; De Backer, J.; Bolmsjö, G. Temperature Measurements during Friction Stir Welding. *Int. J. Adv. Manuf. Technol.* **2017**, *88*, 2899–2908. [[CrossRef](#)]
23. ASTM E384-22; Standard Test Method for Microindentation Hardness of Materials. ASTM International: West Conshohocken, PA, USA, 2022. [[CrossRef](#)]
24. ASTM E8/E8M-22; Standard Test Methods for Tension Testing of Metallic Materials. ASTM International: West Conshohocken, PA, USA, 2022. [[CrossRef](#)]
25. Robitaille, B.; Provencher, P.R.; St-Georges, L.; Brochu, M. Mechanical Properties of 2024-T3 AlClad Aluminum FSW Lap Joints and Impact of Surface Preparation. *Int. J. Fatigue* **2021**, *143*, 105979. [[CrossRef](#)]
26. Nandan, R.; Roy, G.; Lienert, T.; Debroy, T. Three-Dimensional Heat and Material Flow during Friction Stir Welding of Mild Steel. *Acta Mater.* **2007**, *55*, 883–895. [[CrossRef](#)]
27. Verma, S.; Misra, J.P. Effect of Process Parameters on Temperature and Force Distribution during Friction Stir Welding of Armor-Marine Grade Aluminum Alloy. *Proc. Inst. Mech. Eng. Part B J. Eng. Manuf.* **2021**, *235*, 144–154. [[CrossRef](#)]
28. Nadikudi, B.K.B.; Davidson, M.; Akasapu, N.R.; Govindaraju, M. Formability Analysis of Dissimilar Tailor Welded Blanks Welded with Different Tool Pin Profiles. *Trans. Nonferrous Met. Soc. China* **2015**, *25*, 1787–1793. [[CrossRef](#)]
29. Dong, P.; Li, H.; Sun, D.; Gong, W.; Liu, J. Effects of Welding Speed on the Microstructure and Hardness in Friction Stir Welding Joints of 6005A-T6 Aluminum Alloy. *Mater. Des.* **2013**, *45*, 524–531. [[CrossRef](#)]
30. Kumar, A.; Veeresh Nayak, C.; Herbert, M.A.; Rao, S.S. Microstructure and Hardness of Friction Stir Welded Aluminium–Copper Matrix-Based Composite Reinforced with 10 Wt-% SiCp. *Mater. Res. Innov.* **2014**, *18*, S6–S84. [[CrossRef](#)]
31. Darzi Naghibi, H.; Shakeri, M.; Hosseinzadeh, M. Neural Network and Genetic Algorithm Based Modeling and Optimization of Tensile Properties in FSW of AA 5052 to AISI 304 Dissimilar Joints. *Trans. Indian Inst. Met.* **2016**, *69*, 891–900. [[CrossRef](#)]
32. Aydin, H.; Tutar, M.; Durmuş, A.; Bayram, A.; Sayaca, T. Effect of Welding Parameters on Tensile Properties and Fatigue Behavior of Friction Stir Welded 2014-T6 Aluminum Alloy. *Trans. Indian Inst. Met.* **2012**, *65*, 21–30. [[CrossRef](#)]
33. Cabrini, M.; Bocchi, S.; D’Urso, G.; Giardini, C.; Lorenzi, S.; Testa, C.; Pastore, T. Effect of Load on the Corrosion Behavior of Friction Stir Welded AA 7075-T6 Aluminum Alloy. *Materials* **2020**, *13*, 2600. [[CrossRef](#)]
34. Manikandan, P.; Prabhu, T.A.; Manwatkar, S.K.; Rao, G.S.; Murty, S.N.; Sivakumar, D.; Pant, B.; Mohan, M. Tensile and Fracture Properties of Aluminium Alloy AA2219-T87 Friction Stir Weld Joints for Aerospace Applications. *Metall. Mater. Trans. A* **2021**, *52*, 3759–3776. [[CrossRef](#)]
35. Carlone, P.; Astarita, A.; Rubino, F.; Pasquino, N. Microstructural Aspects in FSW and TIG Welding of Cast ZE41A Magnesium Alloy. *Metall. Mater. Trans. B* **2016**, *47*, 1340–1346. [[CrossRef](#)]
36. Topic, I.; Höppel, H.W.; Göken, M. *Deformation Behaviour of Accumulative Roll Bonded and Friction Stir Welded Aluminium Alloys*; Trans Tech Publications: Stafa-Zurich, Switzerland, 2008; Volume 584, pp. 833–839. [[CrossRef](#)]
37. Sun, Y.; Fujii, H.; Takada, Y.; Tsuji, N.; Nakata, K.; Nogi, K. Effect of Initial Grain Size on the Joint Properties of Friction Stir Welded Aluminum. *Mater. Sci. Eng. A* **2009**, *527*, 317–321. [[CrossRef](#)]
38. Aliha, M.; Shahheidari, M.; Bisadi, M.; Akbari, M.; Hossain, S. Mechanical and Metallurgical Properties of Dissimilar AA6061-T6 and AA7277-T6 Joint Made by FSW Technique. *Int. J. Adv. Manuf. Technol.* **2016**, *86*, 2551–2565. [[CrossRef](#)]

Disclaimer/Publisher’s Note: The statements, opinions and data contained in all publications are solely those of the individual author(s) and contributor(s) and not of MDPI and/or the editor(s). MDPI and/or the editor(s) disclaim responsibility for any injury to people or property resulting from any ideas, methods, instructions or products referred to in the content.